

# The XMM-Newton/2dF survey IV. The X-ray spectral properties of the hard sources

I. Georgantopoulos<sup>1</sup>, A. Georgakakis<sup>1</sup>, A. Akylas<sup>1,2</sup>, G.C. Stewart<sup>3</sup>, O. Giannakis<sup>1,2</sup>,  
T. Shanks<sup>4</sup>, S. Kitsionas<sup>1</sup>

<sup>1</sup> *Institute of Astronomy & Astrophysics, National Observatory of Athens, I. Metaxa & B. Pavlou, Penteli, 15236, Athens, Greece*

<sup>2</sup> *Physics Department University of Athens, Panepistimiopolis, Zografos, 15783, Athens, Greece*

<sup>3</sup> *Department of Physics and Astronomy, University of Leicester, Leicester LE1 7RH*

<sup>4</sup> *Physics Department, South Road, Durham, DH1 3LE*

20 November 2018

## ABSTRACT

We present an analysis of the X-ray spectral properties of 61 hard X-ray selected (2–8 keV) sources from the bright ( $f_{2-8\text{keV}} > 10^{-14}$  erg cm<sup>-2</sup> s<sup>-1</sup>) *XMM-Newton*/2dF survey. This comprises of 9 *XMM-Newton* pointings in the North Galactic Pole region ( $\sim 1.6\text{deg}^2$ ) and overlaps with the SDSS, 2QZ and 2dFGRS surveys. Our sources contribute about 50 per cent of the 2–10 keV X-ray background down to the flux limit of  $10^{-14}$  erg cm<sup>-2</sup> s<sup>-1</sup>. The hardness ratio distribution of the sample suggests a deficit of heavily absorbed sources. A spectral fit to the co-added total source spectrum yields a steep photon index,  $\Gamma = 1.83_{-0.05}^{+0.04}$ . All but 8 sources have optical counterparts down to the SDSS photometric limit of  $r \approx 22.5$ . Spectroscopic identifications exist for 34 sources. The vast majority are associated with Broad-Line (BL) AGN (24 sources) while only 7 present narrow or no emission lines. Five sources are probably associated with Galactic stars. Finally, for another 17 probable AGN we present photometric redshifts. The combined spectrum of the 24 spectroscopically identified BL AGN is steep ( $\Gamma = 2.02_{-0.05}^{+0.04}$ ), while that of the 7 AGN, which do not present broad lines is flatter with  $\Gamma = 1.64_{-0.11}^{+0.11}$ . The spectrum of the 8 optically unidentified sources is flat with  $\Gamma \approx 1.1$ . Spectral fits to the individual BL AGN reveal large absorption (rest-frame column density  $> 10^{22}$  cm<sup>-2</sup>) in only two cases. The individual spectra of the NL AGN present significant evidence for even a moderate absorption ( $3 \times 10^{21}$  cm<sup>-2</sup>) in only one case.

## Key words:

galaxies:active-quasars:general-X-rays:general

## 1 INTRODUCTION

Deep *Chandra* surveys have resolved the bulk of the X-ray background in both the soft and the hard energies (Mushotzky et al. 2000; Brandt et al. 2001; Giacconi et al. 2002, Alexander et al. 2003). These surveys detect a heterogeneous population of sources consisting of a mixture of (i) BL AGN (QSOs and Seyfert-1 galaxies), (ii) narrow emission line AGN, (iii) ‘passive’ galaxies with absorption line optical spectra and (iv) optically faint sources ( $I > 24$  mag). It is likely, that both the ‘passive’ galaxies and the optically faint sources may be associated with obscured AGN (see e.g. Moran et al. 2002, Fiore et al. 2003). Nevertheless, deep *Chandra* observations primarily probe the faint ( $< 10^{-16}$  erg cm<sup>-2</sup> s<sup>-1</sup>) X-ray population. At brighter fluxes ( $> 10^{-15}$  erg cm<sup>-2</sup> s<sup>-1</sup>) *Chandra* is limited by its small field of view

( $0.07\text{deg}^2$ ) and cannot provide large samples. However, it is these bright sources that dominate the X-ray Background (XRB) ( $> 50$  per cent, e.g. Boyle et al. 1998). Therefore, to improve our understanding of the sources that make up the XRB, wide area relatively shallow surveys are essential.

*XMM-Newton* with its large field-of-view, high effective area and good positional accuracy provides a step forward in the study of these sources. In this paper, we present the X-ray spectral properties of sources detected in a shallow *XMM-Newton* survey covering a  $\sim 1.6\text{deg}^2$  area near the North Galactic Pole region. In particular, we concentrate on the hard X-ray selected sample (2–8 keV) as these are more typical of the sources contributing to the XRB with its energy density peaking at 30–40 keV. Although extensive surveys have been conducted at these energies by both

the *ASCA* and *BeppoSAX* missions (e.g. Georgantopoulos et al. 1997, Ueda et al. 1998, Giommi et al. 2000), the poor spatial resolution hampered the identification of the optical counterparts. The present data probe a factor of  $\approx 4$  fainter fluxes than the deepest *ASCA* survey (Georgantopoulos et al. 1997) with an order of magnitude better positional accuracy.

Throughout this paper we adopt  $H_0 = 65 \text{ km s}^{-1} \text{ Mpc}^{-1}$  and  $q_0 = 0.3, \Lambda = 0.7$ .

## 2 XMM-NEWTON/2DF SURVEY OVERVIEW

The X-ray sample used in the present study is compiled from the *XMM-Newton*/2dF survey. This is a wide area ( $\sim 4 \text{ deg}^2$ ) shallow (2–10 ks per pointing) survey carried out by the *XMM-Newton* near the North and the South Galactic Pole regions. The data reduction, source extraction, flux estimation and catalogue generation are described in detail by Georgakakis et al. (2003, 2004). In the present study we concentrate on the North Galactic Pole F864 region. This is because of the wealth of follow-up observations (optical photometry and spectroscopy) available for these fields.

The *XMM-Newton*/2dF survey F864 region overlaps with the Sloan Digital Sky Survey, SDSS, (York et al. 2000). The SDSS is an on-going imaging and spectroscopic survey that aims to cover about  $10\,000 \text{ deg}^2$  of the sky. Photometry is performed in 5 bands (*ugriz*; Fukugita et al. 1996; Stoughton et al. 2002) to the limiting magnitude  $g \approx 23 \text{ mag}$ , providing a uniform and homogeneous multi-color photometric catalogue. The SDSS spectroscopic observations will obtain spectra for over 1 million objects, including galaxies brighter than  $r = 17.7 \text{ mag}$ , luminous red galaxies to  $z \approx 0.45$  and colour selected QSOs (York et al. 2000; Stoughton et al. 2002). In the present study we use data from the Early Data Release (EDR; Stoughton et al. 2002).

In addition to the SDSS the F864 region overlaps with the recently completed 2dF Galaxy Redshift Survey (2dFGRS<sup>\*</sup>; Colless et al. 2001; Colless et al. 2003) and the 2dF QSO Redshift Survey (2QZ<sup>†</sup>; Croom et al. 2001). Both the 2dFGRS and 2QZ are large-scale spectroscopic campaigns that fully exploit the capabilities of the 2dF multi-fibre spectrograph on the 4 m Anglo-Australian Telescope (AAT). These projects provide high quality spectra, redshifts and spectral classifications for 220 000  $bj < 19.4 \text{ mag}$  galaxies and 23 000 optically selected  $bj < 20.85 \text{ mag}$  QSOs. Moreover, the central region of the F864 survey have been observed by the *ROSAT* satellite (Shanks et al. 1991, Georgantopoulos et al. 1996).

## 3 THE X-RAY DATA

The EPIC (European Photon Imaging Camera; Strüder et al. 2001 and Turner et al. 2001) cameras were operated in full frame mode with the thin filter applied. The *XMM-Newton* data have been analysed using the Science Analysis Software

(SAS 5.3). Event files for the PN and the two MOS detectors have been produced using the EPCHAIN and EMCHAIN tasks of SAS respectively. The event files were screened for high particle background periods by rejecting periods with 0.5–10 keV count rates higher than 25 and 15 cts/s for the PN and the two MOS cameras respectively. These criteria exclude one field (F864–4) from the analysis that suffered by significantly elevated and flaring particle background. The resulting area covered by the survey is  $1.6 \text{ deg}^2$ . The PN and MOS good time intervals for the remaining pointings are shown in Table 1. The differences between the PN and MOS exposure times are due to varying start and end times of individual observations. Only events corresponding to patterns 0–4 for the PN and 0–12 for MOS have been kept.

In order to increase the signal-to-noise ratio and to reach fainter fluxes the PN and the MOS event files have been combined into a single event list using the MERGE task of SAS. Images have been extracted in the spectral bands 0.5–8 (total), 0.5–2 (soft) and 2–8 keV (hard) for both the merged and the individual PN and MOS event files. We use the more sensitive (higher S/N ratio) merged image for source extraction and flux estimation, while the individual PN and MOS images are used to calculate hardness ratios. This is because the interpretation of hardness ratios is simplified if the extracted count rates are from one detector only. Exposure maps accounting for vignetting, CCD gaps and bad pixels have been constructed for each spectral band. In the present study the source detection is performed on the 2–8 keV image using the EWAVELET task of SAS with a detection threshold of  $6\sigma$ . A total of 61 X-ray sources have been detected to the limit  $f_X(2 - 8 \text{ keV}) \approx 10^{-14} \text{ erg s}^{-1} \text{ cm}^{-2}$ . Integration of the logN-logS derived by Baldi et al. (2002) to the above flux limit gives, shows that about 50 per cent of the XRB is resolved at these energies.

Count rates in the merged (PN+MOS) images as well as the individual PN and MOS images are estimated within an 18 arcsec aperture. For the background estimation we use the background maps generated as a by-product of the EWAVELET task of SAS. A small fraction of sources lie close to masked regions (CCD gaps or hot pixels) on either the MOS or the PN detectors. This may introduce errors in the estimated source counts. To avoid this bias, the source count rates (and hence the hardness ratios and the flux) are estimated using the detector (MOS or PN) with no masked pixels in the vicinity of the source.

We convert counts to flux assuming a power-law spectrum with  $\Gamma = 1.7$  and Galactic absorption  $N_H = 2 \times 10^{20} \text{ cm}^{-2}$  appropriate for the F864 fields (Dickey & Lockman 1990). Note that a  $\Gamma = 1.7$  photon index provides a reasonable representation of the typical source spectrum being intermediate between the steep BL AGN and the unidentified flatter sources (see section 5.3). The mean ECF for the mosaic of all three detectors is estimated by weighting the ECFs of individual detectors by the respective exposure time. For the encircled energy correction, accounting for the energy fraction outside the aperture within which source counts are accumulated, we adopt the calibration

\* <http://msowww.anu.edu.au/2dFGRS/>

† <http://www.2dfquasar.org>

Field Name	RA (J2000)	Dec (J2000)	PN exp. time (sec)	MOS exp. time (sec)
F864-1	13 <sup>h</sup> 41 <sup>m</sup> 24.0 <sup>s</sup>	+00°24′00″	5779	9974
F864-2	13 <sup>h</sup> 43 <sup>m</sup> 00.0 <sup>s</sup>	+00°24′00″	2958	6586
F864-3	13 <sup>h</sup> 44 <sup>m</sup> 36.0 <sup>s</sup>	+00°24′00″	2187	7727
F864-4	13 <sup>h</sup> 41 <sup>m</sup> 24.0 <sup>s</sup>	+00°00′00″	–	–
F864-5	13 <sup>h</sup> 43 <sup>m</sup> 00.0 <sup>s</sup>	+00°00′00″	1693	4447
F864-6	13 <sup>h</sup> 44 <sup>m</sup> 36.0 <sup>s</sup>	+00°00′00″	2766	6493
F864-7	13 <sup>h</sup> 41 <sup>m</sup> 24.0 <sup>s</sup>	−00°24′00″	3459	7139
F864-8	13 <sup>h</sup> 43 <sup>m</sup> 24.0 <sup>s</sup>	−00°24′00″	2109	7276
F864-9	13 <sup>h</sup> 44 <sup>m</sup> 36.0 <sup>s</sup>	−00°24′00″	4545	8330

**Table 1.** Observing log of the *XMM-Newton*/2dF survey F864 region

given by the *XMM-Newton* Calibration Documentation <sup>‡</sup>. These studies use both PN and MOS observations of point sources to formulate the *XMM-Newton* PSF for different energies and off-axis angles. In particular, a King profile is fit to the data with parameters that are a function of both energy and off-axis angle.

#### 4 THE OPTICAL COUNTERPARTS

The SDSS optical photometric catalogue is used to optically identify the hard selected sample by estimating the probability,  $P$ , a given candidate is chance coincidence (Downes et al. 1986). Of the 61 hard X-ray sources we propose 49 candidate optical identifications with  $P < 0.015$ ; 8 sources have no optical counterpart. 4 sources have a probability higher than 0.015 of being spurious and thus they are less secure identifications. The probability depends on both the separation of the optical counterpart from the X-ray centroid and the surface density of the optical sources at the given magnitude (see Georgakakis et al. 2004 for details). To estimate the fraction of spurious identifications in our sample we randomise the X-ray source positions and re-estimate the number of optical counterparts. This is repeated 100 times. We find a spurious identification rate of  $\approx 6$  per cent or about 4 spurious optical counterparts out of the 61 sources.

The catalogue of the X-ray sources is given in Table 2. Optical spectroscopic information are available for 34 out of the 61 sources. These contribute about 30 per cent of the XRB in the 2–8 keV energy band. A total of 21 sources have redshifts and optical classifications from our own spectroscopic campaign using the 2dF (Georgantopoulos et al. 2004 in preparation). The remaining sources have spectroscopic data from the 2QZ, 2dFGRS and the SDSS surveys. The spectroscopically identified sample comprises: (i) 24 sources with broad optical emission lines (BL AGN). (ii) five sources with narrow lines (NL) (iii) two with absorption lines (AL) As all the NL/AL objects have luminosities in excess of  $10^{42}$  erg s<sup>−1</sup>, these are most probably AGN. (iv) three stars; note that closer inspection of the (low signal-to-noise) spectrum of source #2 which is classified as a star by the 2QZ survey, leaves open the possibility that this is associated with

a galaxy at a redshift of  $z=0.243$ . We also note that two additional sources for which no spectroscopic information is available (#1 and #26) are candidate stars on the basis of their low  $f_x/f_o$  ratio and optical colours (for the latter see e.g. Hatziminaoglou, Mathez & Pello 2000). In addition, to the spectroscopic redshifts, we have estimated photometric redshifts, using the multiwaveband coverage of the SDSS, for 6 X-ray sources which are most probably QSOs as they have point-like optical profile and high X-ray to optical flux ratio. The photometric redshift technique is fully described in Kitsionas et al. (in preparation) and Hatziminaoglou et al. (2000). Note that point-like sources with a determined photometric redshift of  $z < 0.4$ , are likely to present large uncertainties in their redshift (Kitsionas et al. in preparation). For 11 sources (#4, 6, 13, 14, 15, 18, 22, 24, 46, 47, 60) which are optically extended (most have also red colours), we have used the photometric redshifts provided by SDSS which are based on galaxy templates (Csabai et al. 2003).

As a fraction of the spectroscopic identifications come from the 2QZ survey, there may be a bias towards the detection of a high number of QSOs among our identified sources. We plot the column density and flux distributions, in order to further understand any possible biases introduced. The *observer’s frame* column density is derived from the hardness ratios as described in section 5.1. Indeed, from Fig. 1, we see that the unidentified sources are in general harder. This is not surprising as many of our optical identification are based on the SDSS and 2QZ surveys which are designed to detect UV excess selected QSOs most of which do not show strong absorption in X-rays. In Fig. 2, we present the flux distribution, again separating the spectroscopically identified and the unidentified sources. Both the spectroscopically identified and unidentified sources appear to sample the whole flux range. However, at the faintest flux bin, there are more unidentified sources.

In Fig. 3 we plot the redshift distribution of the BL (24) and AL/NL (7) AGN. The NL AGN are preferably detected at low redshift in agreement with the findings of other hard X-ray surveys (e.g. Brusa et al. 2003). Fig. 4 shows the colour-colour plot for the optically identified hard X-ray sources. A striking result from this Figure is the significant number of red ( $g - r > 0.5$ ) sources with extended optical profiles suggesting relatively low- $z$  galaxies. Fig. 4 suggests that these sources are a non-negligible mode of the hard X-ray selected population to the limit of our survey.

<sup>‡</sup> [http://xmm.vilspa.esa.es/external/xmm\\_sw\\_cal/calib/documentation.shtml#XRT](http://xmm.vilspa.esa.es/external/xmm_sw_cal/calib/documentation.shtml#XRT)

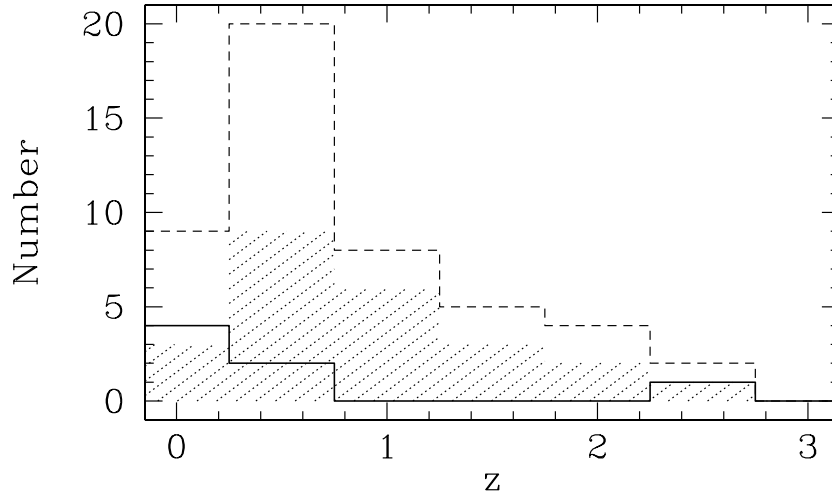


**Figure 3.** The redshift distributions of the spectroscopically identified BL AGNs (hatched histogram), NL/AL AGN (solid line) and the full sample i.e. including photometric redshifts (dashed line).

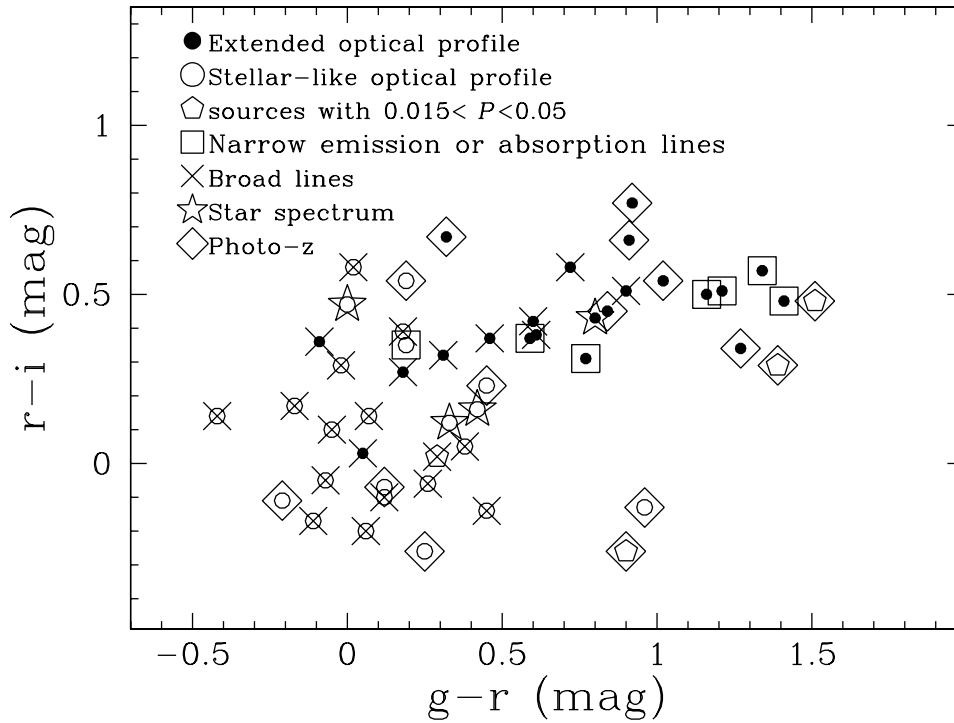


**Figure 4.**  $g-r$  against  $r-i$  colour-colour diagram for the hard X-ray selected sample. Filled and open circles on top of a symbol correspond to the sources with stellar-like and extended optical morphology according to the SDSS. The pentagon is for sources with higher probability of being spurious alignments ( $0.015 < P < 0.05$ ). Open squares are for NL/AL, crosses are BL AGNs and stars correspond to spectroscopically confirmed stars. The diamonds correspond to sources with photometric redshift estimates.

**Table 2.** Optical and X-ray properties of the sample

#	$\alpha_X$ (J2000)	$\delta_X$ (J2000)	count rate <sup>a</sup>	flux <sup>b</sup>	exp. time <sup>c</sup>	$P$ (%)	$\delta r$ (arcsec)	$g$ (mag)	optical class	$z$	class
(1)	(2)	(3)	(4)	(5)	(6)	(7)	(8)	(9)	(10)	(11)	(12)
1	13 45 15.0	-00 00 48	8 ± 3.9	9.78 ± 2.04	6871	< 0.01	0.3	15.44	point-like	0.000	STAR <sup>f</sup>
2	13 45 10.4	+00 18 51	6.8 ± 4	5.14 ± 1.43	9717	0.19	1.6	19.17	extended	0.000	STAR? <sup>g</sup>
3	13 45 09.8	+00 20 52	11.1 ± 4.49	15.7 ± 2.32	8137	0.82	2.4	19.54	extended	0.370	NL
4	13 45 08.5	+00 22 27	1 ± 2.6	2.52 ± 1.06	11523	1.19	1.9	21.05	extended	0.415	photo-z <sup>e</sup>
5	13 45 08.0	-00 05 29	12.7 ± 4.6	10.3 ± 2.05	7183	0.26	2.2	19.77	extended	0.730	BL
6	13 45 07.4	+00 04 09	6.7 ± 3.4	5.66 ± 1.56	7724	0.67	2.6	19.52	extended	0.553	photo-z <sup>e</sup>
7	13 45 01.7	-00 24 02	5.5 ± 1.9	3.77 ± 0.83	16074	0.01	0.8	17.38	point-like	0.000	STAR
8 <sup>d</sup>	13 44 59.5	-00 16 01	14.7 ± 1.5	27.5 ± 2.89	9824	0.05	1.8	17.52	point-like	0.245	BL
9	13 44 58.5	+00 16 23	5.1 ± 3.6	3.13 ± 1.21	10167	0.26	2.9	18.02	extended	0.145	NL
10	13 44 58.0	-00 36 00	12.5 ± 3.8	8.69 ± 1.64	8110	1.36	4.4	19.38	extended	0.465	BL
11 <sup>d</sup>	13 44 52.9	+00 05 21	20.2 ± 1.9	37.8 ± 3.54	9789	0.01	0.7	16.32	extended	0.087	BL
12	13 44 52.3	-00 36 54	4.2 ± 2.7	2.78 ± 1.8	5895	0.77	3.3	20.3	point-like	0.810	photo-z
13	13 44 51.6	-00 23 01	4.49 ± 1.6	2.5 ± 0.65	18932	0.30	1.4	19.64	extended	0.261	photo-z <sup>e</sup>
14	13 44 47.0	-00 30 09	3 ± 1.6	2.45 ± 0.74	15454	0.67	1.1	20.18	extended	0.529	photo-z <sup>e</sup>
15	13 44 44.1	-00 19 30	2 ± 1.3	1.67 ± 0.62	17078	4.87	2.6	22.28	extended	0.779	photo-z <sup>e</sup>
16 <sup>d</sup>	13 44 38.9	-00 11 01	5.7 ± 1.19	10.6 ± 2.32	6173	-	-	-	-	-	-
17	13 44 36.4	+00 33 24	11.1 ± 4.49	4.71 ± 1.45	9018	1.38	3.7	20.16	point-like	1.430	BL
18	13 44 33.5	-00 24 55	4.1 ± 1.4	3.35 ± 0.69	20492	0.32	0.8	22.91	extended	0.511	photo-z <sup>e</sup>
19	13 44 25.3	-00 18 27	5.2 ± 1.8	3.7 ± 0.85	14566	0.34	1.5	21.71	point-like	1.970	BL
20 <sup>d</sup>	13 44 24.7	-00 13 08	2.8 ± 0.9	5.26 ± 1.65	7915	2.19	4.7	20.41	point-like	1.110	BL
21 <sup>d</sup>	13 44 22.1	-00 34 20	2.9 ± 0.9	5.36 ± 1.61	8539	0.10	1.3	18.2	extended	0.217	NL
22	13 44 20.2	+00 04 17	5.4 ± 2.6	4.76 ± 1.09	12779	2.45	3.3	19.98	extended	0.302	photo-z <sup>e</sup>
23	13 44 20.1	-00 31 11	5 ± 2.1	4.56 ± 1.08	11903	0.02	0.5	20.33	extended	0.680	BL
24 <sup>d</sup>	13 44 14.2	+00 16 41	29.8 ± 2.39	55.8 ± 4.42	8546	0.06	1.1	19.34	extended	0.706	photo-z <sup>e</sup>
25	13 44 04.7	-00 09 23	7.8 ± 4.4	6.96 ± 1.83	6549	-	-	-	-	-	-
26	13 43 52.5	-00 04 33	14.4 ± 5.2	8.95 ± 1.91	7327	0.97	8.2	16.99	point-like	-0.000	STAR <sup>f</sup>
27 <sup>d</sup>	13 43 51.1	+00 04 38	3.3 ± 1	6.25 ± 1.84	6311	0.16	3.4	16.75	extended	0.074	BL
28 <sup>d</sup>	13 43 47.5	+00 20 21	6.6 ± 1.3	12.4 ± 2.44	5940	0.37	2.6	18.14	extended	0.240	AL
29 <sup>d</sup>	13 43 31.6	+00 24 49	2.39 ± 0.7	4.56 ± 1.31	9978	0.82	3.4	20.27	point-like	1.300	photo-z
30 <sup>d</sup>	13 43 29.2	+00 01 35	3.7 ± 1.5	6.94 ± 2.85	5307	0.75	2.2	21.04	point-like	2.347	NL
31	13 43 23.8	+00 12 21	8.4 ± 4	9.13 ± 1.93	6390	0.26	3.3	18.31	point-like	0.874	BL
32	13 43 07.9	+00 27 19	2.2 ± 1.6	2.21 ± 0.73	13999	0.42	2.4	20.87	point-like	2.310	BL
33	13 43 01.5	+00 26 34	5.6 ± 2	4.94 ± 0.95	14735	0.75	2.2	20.42	point-like	1.500	photo-z
34 <sup>d</sup>	13 42 56.6	+00 00 57	8.1 ± 1.3	15.2 ± 2.49	10078	0.06	1.3	18.77	point-like	0.804	BL
35	13 42 55.5	+00 06 36	11.2 ± 4.4	7.87 ± 2.08	7602	0.13	1.5	19.33	extended	0.436	BL
36 <sup>d</sup>	13 42 46.3	-00 35 44	6 ± 1.7	11.3 ± 3.19	6054	0.01	0.5	18.14	point-like	0.787	BL
37	13 42 42.8	+00 32 23	7.2 ± 3.2	4.74 ± 2.11	7858	-	-	-	-	-	-

<sup>a</sup> 2-8 keV count rate in cts s<sup>-1</sup>

<sup>b</sup> 2-8 keV flux in units of 10<sup>-14</sup> erg s<sup>-1</sup> cm<sup>-2</sup>

<sup>c</sup> total exposure time in the 2-8 keV band from the merged PN+MOS image in seconds

<sup>d</sup> count rate and flux is from MOS

<sup>e</sup> photometric redshifts are from the SDSS catalogue

<sup>f</sup> X-ray/optical properties indicate Galactic star but spectroscopy is not available

<sup>g</sup> The identification from 2QZ gives a star. However, the spectrum may be suggesting a galaxy at z=0.243

## 5 X-RAY SPECTRAL ANALYSIS

### 5.1 Hardness ratios

In Fig. 5 we plot the hardness ratio as a function of flux. The column densities are derived from the observed hardness ratio using the PIMMS software assuming a power-law spectrum with  $\Gamma = 1.9$ . Error bars correspond to the 68 per cent confidence level. For clarity we plot the error bars only in the cases where the source contains more than 5 net counts in both energy bands. As it was previously explained in section 3, the hardness ratios are estimated from either the MOS or the PN detectors. As the MOS has a lower effective area at low energies, compared to the PN, the same

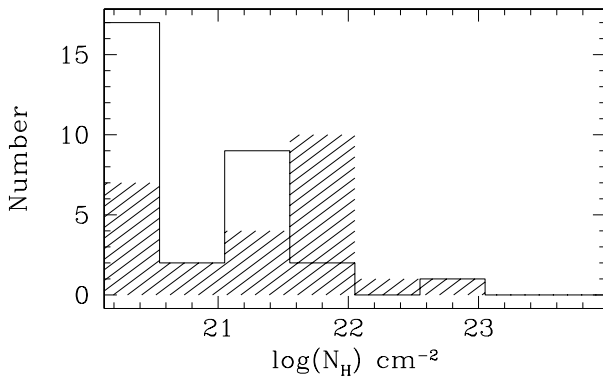
hardness ratio corresponds to different X-ray spectral properties (e.g.  $\Gamma$ ,  $N_H$ ).

In Fig. 5 we also plot the lines corresponding to an absorbing column of  $N_H = 10^{21}$  and  $10^{22}$  cm<sup>-2</sup>, assuming a power-law spectrum with a photon index of  $\Gamma = 1.9$  for the MOS and PN. Note that the lines for the MOS and the PN are identical for high absorbing columns  $N_H > 5 \times 10^{21}$  cm<sup>-2</sup>. Although the sources span a large range of hardness ratios, most cluster around soft values: the average hardness ratio corresponds to a spectrum  $N_H \sim 3 \times 10^{21}$  cm<sup>-2</sup> (for  $\Gamma = 1.9$ ).

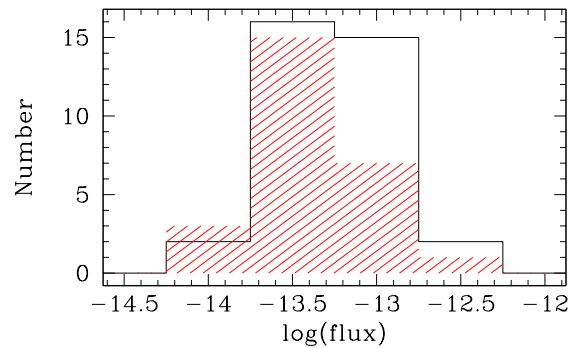
The *observer's frame* column density distribution was presented in Fig.1. The column densities estimated there represent only a lower limit to the true, *rest-frame* column

**Table 2** – *continued*

#	$\alpha_X$ (J2000)	$\delta_X$ (J2000)	count rate <sup>a</sup>	flux <sup>b</sup>	exp. time <sup>c</sup>	$P$ (%)	$\delta r$ (arcsec)	$g$ (mag)	optical class	$z$	class
(1)	(2)	(3)	(4)	(5)	(6)	(7)	(8)	(9)	(10)	(11)	(12)
38	13 42 34.5	+00 32 23	$2.9 \pm 2.7$	$4.02 \pm 1.43$	6883	1.32	2.4	20.98	point-like	1.950	photo-z
39 <sup>d</sup>	13 42 33.7	-00 11 49	$5.4 \pm 2.1$	$10.2 \pm 3.87$	3182	0.03	0.9	19.06	point-like	0.516	BL
40	13 42 12.0	+00 29 49	$5.2 \pm 2.8$	$3.99 \pm 1.33$	7603	0.60	2	20.41	extended	0.570	BL
41 <sup>d</sup>	13 42 11.7	-00 23 32	$4.2 \pm 1.3$	$7.76 \pm 2.5$	5379	–	–	–	–	–	–
42	13 41 47.8	+00 31 08	$2.2 \pm 1.6$	$2.84 \pm 0.9$	12635	0.28	1.4	20.56	point-like	1.335	BL
43	13 41 42.9	+00 12 39	$6.7 \pm 2.6$	$4.5 \pm 1.25$	9093	0.07	1.1	19.83	point-like	0.788	BL
44	13 41 40.5	+00 15 44	$4.3 \pm 1.9$	$3.55 \pm 0.97$	12732	0.80	3.3	18.59	extended	0.254	AL
45 <sup>d</sup>	13 41 38.1	+00 27 01	$1.3 \pm 0.4$	$2.44 \pm 0.79$	18460	–	–	–	–	–	–
46	13 41 34.4	+00 28 08	$2.39 \pm 1.19$	$2.01 \pm 0.61$	20020	0.22	1.2	20.26	extended	0.676	photo-z <sup>e</sup>
47	13 41 28.4	-00 31 20	$14.3 \pm 3.4$	$13.5 \pm 1.73$	11128	0.03	0.3	20.63	extended	0.619	photo-z <sup>e</sup>
48	13 41 27.8	+00 32 13	$3 \pm 1.8$	$2.98 \pm 0.85$	14784	0.57	2	21.71	point-like	1.764	BL
49	13 41 27.2	+00 14 14	$10.1 \pm 2.5$	$6.06 \pm 1.17$	12444	0.01	0.4	19.45	point-like	1.698	BL
50	13 41 27.1	+00 23 28	$2.39 \pm 1.1$	$1.7 \pm 0.5$	24650	0.03	0.3	21.38	point-like	0.120?	photo-z
51	13 41 23.8	+00 22 05	$1 \pm 0.9$	$1.65 \pm 0.51$	24035	–	–	–	–	–	–
52	13 41 22.5	+00 28 26	$2.7 \pm 1.19$	$1.48 \pm 0.54$	21578	0.60	2	21.9	point-like	2.250	photo-z
53	13 41 21.6	-00 13 51	$7.5 \pm 3.4$	$4.42 \pm 1.33$	8937	0.47	3.9	19.24	point-like	0.736	BL
54	13 41 18.1	-00 23 21	$14.1 \pm 2.7$	$12.2 \pm 1.3$	17665	0.48	2.6	19.63	extended	0.423	BL
55	13 41 17.1	+00 21 51	$3.7 \pm 1.19$	$2.68 \pm 0.59$	23633	0.22	1.5	21.17	extended	0.721	BL
56	13 41 15.0	+00 19 46	$1.6 \pm 1.1$	$1.45 \pm 0.54$	20778	–	–	–	–	–	–
57	13 41 02.9	+00 15 48	$5.4 \pm 2.2$	$4.05 \pm 0.99$	13280	0.07	1.1	19.62	point-like	1.038	BL
58	13 40 56.5	+00 31 58	$3.5 \pm 1.9$	$3.76 \pm 0.95$	13371	< 0.01	1.6	16.9	point-like	0.000	STAR
59	13 40 50.2	+00 15 54	$6.1 \pm 2.5$	$5.03 \pm 1.16$	11240	–	6.4	–	–	–	–
60	13 40 45.2	-00 24 02	$15.6 \pm 4.1$	$9.48 \pm 1.61$	10164	4.03	3.5	20.18	extended	0.215	photo-z <sup>e</sup>
61	13 40 38.7	+00 19 19	$8.6 \pm 2.8$	$8.8 \pm 1.43$	10983	0.11	1	19.62	extended	0.244	NL

<sup>a</sup> 2-8 keV count rate in cts s<sup>-1</sup><sup>b</sup> 2-8 keV flux in units of 10<sup>-14</sup> erg s<sup>-1</sup> cm<sup>-2</sup><sup>c</sup> total exposure time in the 2-8 keV band from the merged PN+MOS image in seconds<sup>d</sup> count rate and flux is from MOS<sup>e</sup> photometric redshifts are from the SDSS catalogue<sup>f</sup> X-ray/optical properties indicate Galactic star but spectroscopy is not available**Figure 1.** The *observer's frame* column density distribution for the spectroscopically unidentified (open) and identified (hatched) samples.

densities. The rest-frame column density is higher than the observed one as the *k*-effect shifts the absorption turn-over at lower energies. The relation between the intrinsic rest-frame and observer's frame column density scales approximately as  $(1+z)^{2.7}$  (Barger et al. 2002). The Galactic column

**Figure 2.** Flux (2-8 keV) distribution of the spectroscopically identified (hatched) and unidentified (open) sources.

density of  $2 \times 10^{20}$  cm<sup>-2</sup> has been subtracted before applying the above correction. In Fig. 6 (upper panel) we show the *rest-frame* column density distribution for the 31 AGN which have a spectroscopic redshift: the unshaded and the hatched histograms represent the BL and NL/AL AGN respectively. It appears that there is a small fraction of heavily

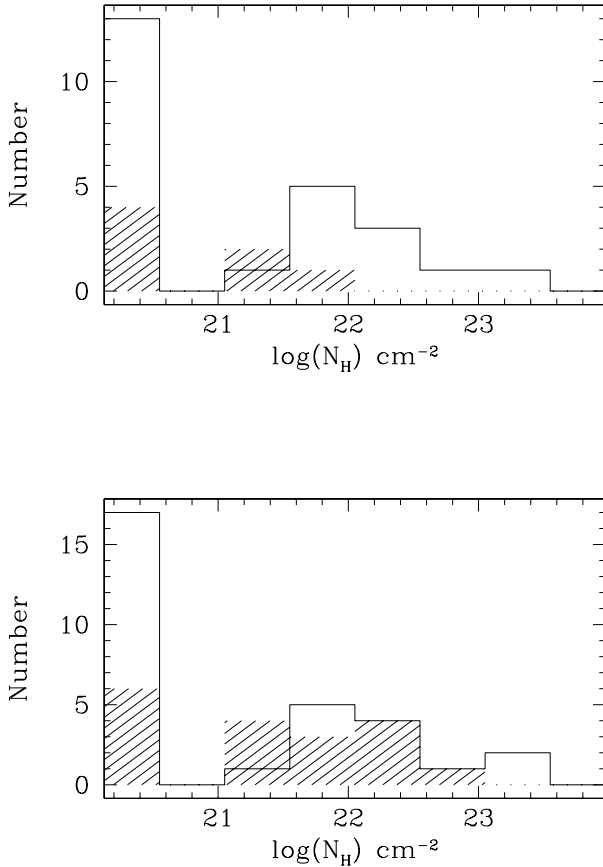


**Figure 6.** Upper panel: The *rest-frame* column density distribution for the spectroscopically identified 24 BL (unshaded) and the 7 NL/AL (hatched) subsamples. Lower panel: The *rest-frame* column density distribution for all AGN (including those with photometric redshifts) i.e. the 30 BL and point-like sources (open) and the 18 NL/AL AGN and extended sources (shaded).

absorbed ( $N_{\text{H}} > 10^{22} \text{ cm}^{-2}$ ) BL AGN. In the whole sample, there are 11 sources whose 90 per cent lower-limit of the hardness ratio corresponds to an observer’s frame column density  $N_{\text{H}} > 10^{21} \text{ cm}^{-2}$ . Two of them are spectroscopically identified as BL AGN while one source is most probably a BL AGN on the basis of its stellar like optical morphology and high  $f_x/f_o$  ratio. Interestingly, the majority of the NL AGN present soft hardness ratios i.e. low column densities consistent with the Galactic. However, as the hardness ratio analysis provides only a rough estimate of the X-ray spectral properties, in the next section we attempt to constrain the column densities via proper spectral fittings.

## 5.2 Spectral fits to individual sources

Here, we attempt to derive the spectral properties of a subsample of interesting sources. More specifically, we derive the spectral fits for the three QSOs which have high hardness ratio values (i.e. indicating hard spectra) as well as for all seven NL/AL AGN. For the X-ray spectral analysis the

source counts are extracted using a radius of 18 arcsec. The background spectrum is estimated from image regions free from sources. Response matrices and auxiliary files are generated using the SAS tasks RMFGEN and ARFGEN respectively. Spectral fits use the XSPEC v11.2 software. The quoted errors correspond to the 90 per cent confidence level.

First, we attempt to constrain the intrinsic column densities of the 3 BL AGN above, via proper spectral fitting, using the XSPEC software. We perform the spectral fitting in the 0.3-8 keV band where the instrument calibration is well known. As our sources are faint, we use the C-statistic (Cash 1979) which does not require for the binning of the data. However, the C-statistic does not allow for the derivation of the goodness of fit probability unlike the  $\chi^2$  statistic. We fit a power-law model absorbed by the Galactic column ( $N_{\text{H}} = 2 \times 10^{20} \text{ cm}^{-2}$ ) and an additional intrinsic column density. The power-law slope is fixed to  $\Gamma = 1.9$  with the only free parameters being the normalization and the intrinsic column density. The results are presented in Table 3. Large column densities are found in the cases of the two spectroscopically confirmed BL AGN: #19 and #10 having intrinsic columns of  $3 \times 10^{22}$  and  $10^{23} \text{ cm}^{-2}$  at redshifts  $z \approx 2$  and  $z \approx 0.5$  respectively. The first QSO presents UV excess having  $U - B \approx -0.6$  while the second one has  $U - B \approx +0.6$  and is extended in the SDSS images. In the third case, #52, a candidate QSO with a photometric redshift  $z=2.25$ , we find a 90 per cent upper limit of  $8 \times 10^{21} \text{ cm}^{-2}$  for the intrinsic column density. In Fig. 7 we present as an example the spectral fit to one of the BL QSOs which present significant absorption (#19 at  $z=1.970$ ). The spectrum is grouped so that it contains a minimum number of 5 photons per bin.

In addition, we present the spectral fits to the 7 NL/AL AGN. We fit the same spectral model as above. The results are presented in Table 3. In most cases we find little evidence for large rest-frame column densities ( $> 10^{21} \text{ cm}^{-2}$ ). Object #30 at a redshift of  $z = 2.35$  is associated with a NL QSO in the optical which has been detected in previous *ROSAT* and *ASCA* surveys (Almaini et al. 1995, Georgantopoulos et al. 1999). The *ASCA* spectrum of this object can be represented with a flat power-law ( $\Gamma \approx 1.5$ ) suggesting some level of obscuration (Georgantopoulos et al. 1999). Unfortunately, the *XMM-Newton* spectrum has limited photon statistics, failing to provide additional clues on the nature of this object. Indeed, when we fit a power-law spectrum to the data fixing the column density to the Galactic we obtain  $\Gamma = 1.77 \pm 0.36$  in agreement with the *ASCA* best-fit values.

## 5.3 The average source spectrum

Next we present an analysis of the average source spectrum in the 0.3-8 keV band by co-adding the photons from all 61 sources in the observer’s frame. About 15 of the 61 sources either lie close to gaps or bad pixels on the PN or outside the PN field of view. These sources are still detected at a high confidence level on the MOS detectors which is less affected by CCD gaps. To improve the statistical significance of our results in the analysis that follows we use the MOS data only. We note however, that using the PN detector does not modify our conclusions. The vignetting and PSF corrections were applied by creating individual auxiliary files for each source. The auxiliary files were then combined using the AD-DARF task in FTOOLS. The data have been binned to give at

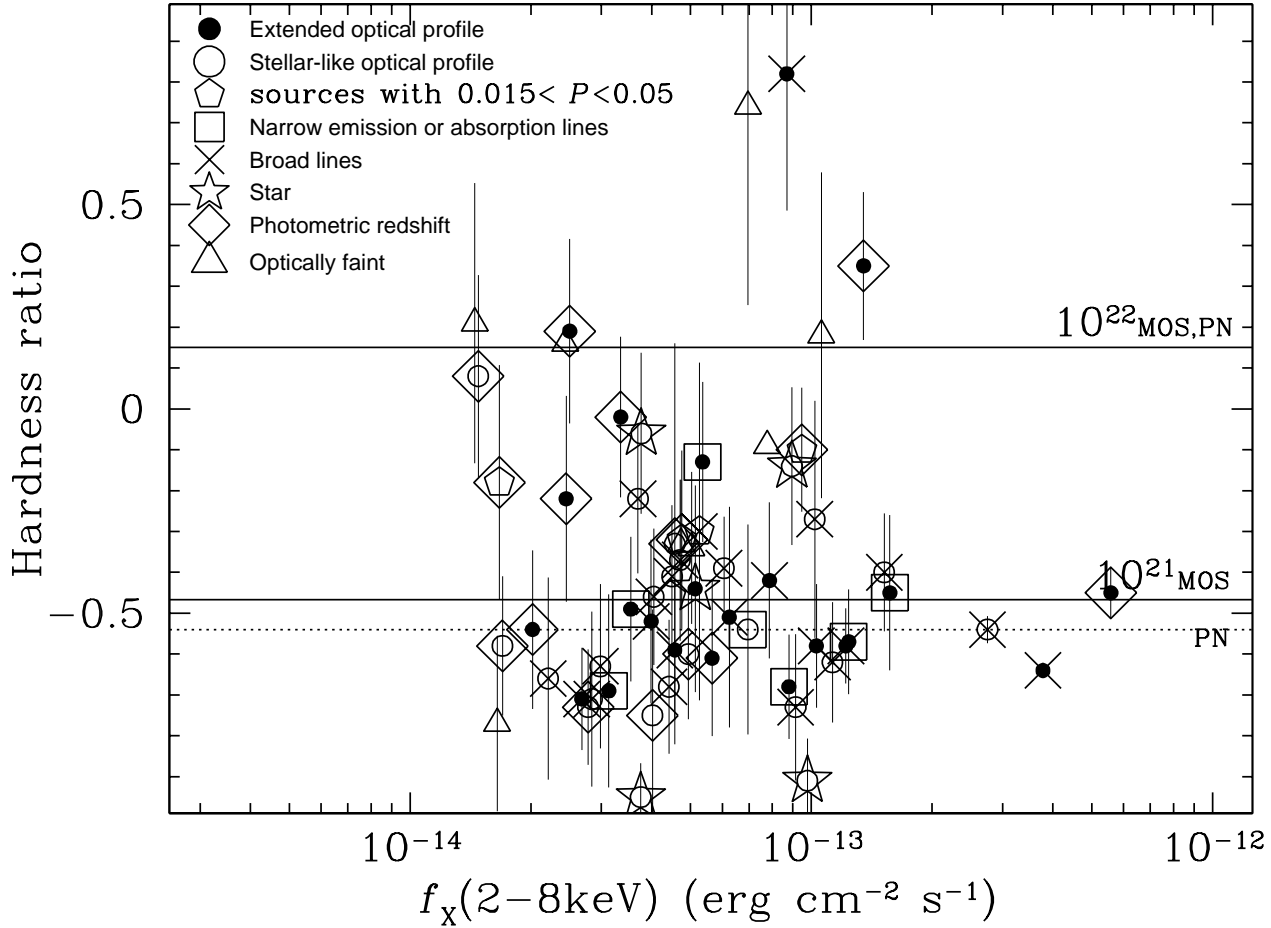


**Figure 5.** The hardness ratio defined as  $h - s / h + s$  ( $h$  and  $s$  are the count rates in the 0.5–2 and 2–8 keV bands respectively) as a function of the 2–8 keV flux. For clarity we do not plot the errors for the sources with very large error bars and thus practically unconstrained hardness ratios (see text). Symbols as in Fig. 4. Sources with no optical counterpart that are absent from Fig. 4 are plotted as triangles. The horizontal lines denote spectra with a photon index of  $\Gamma = 1.9$  absorbed by columns of  $10^{21}$  and  $10^{22}$   $\text{cm}^{-2}$ .

**Table 3.** Spectral fits to individual sources

Object	type	$z$	$L_x^1$	$N_H^2$	Counts <sup>3</sup>
3	NL	0.370	44.0	$0.3^{+0.1}_{-0.1}$	153
9	NL	0.145	42.8	$< 0.03$	95
10	BL	0.465	43.6	$34^{+30}_{-20}$	39
19	BL	1.970	45.0	$3^{+3}_{-2}$	73
21	NL	0.218	42.9	$< 0.4$	56
28	AL	0.240	43.6	$< 0.1$	140
30	NL	2.350	45.7	$< 0.6$	58
44	AL	0.254	43.1	$< 0.2$	107
52	BL	2.250	44.7	$< 0.8$	34
61	NL	0.244	43.6	$< 0.01$	223

<sup>1</sup> Logarithm of the absorbed Luminosity in the 0.5–8 keV band ( $\text{erg s}^{-1}$ )

<sup>2</sup> Intrinsic rest-frame column density in units of  $10^{22}$   $\text{cm}^{-2}$

<sup>3</sup> Sum of MOS and PN counts in the 0.5–8 keV band

least 20 counts per bin so that Gaussian statistics apply. We fit a single power-law model to the data. The spectral fit results are presented in Table 4.

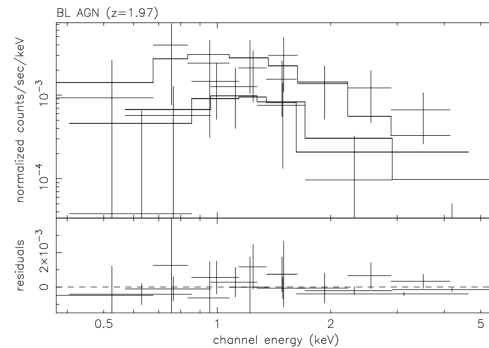


**Figure 7.** The best-fit model and residuals to the spectrum of a BL AGN which presents a significant obscuring column (#19 at  $z=1.97$ ).

The co-added spectrum of all 61 sources is best fitted by a power-law spectral energy distribution  $\Gamma = 1.83^{+0.04}_{-0.05}$ , much steeper than the spectrum of the XRB at these energies. This spectrum is dominated by several bright sources. Excluding the 9 sources which contribute about 60 per cent



**Table 4.** Spectral fits to the co-added source spectra

Sample	No	$\Gamma$	$\chi^2/\text{dof}$
All	61	$1.83^{+0.04}_{-0.05}$	235/238
All excl. 9 bright sources	52	$1.49^{+0.06}_{-0.06}$	126/132
BL AGN	24	$2.02^{+0.04}_{-0.05}$	247/151
BL AGN (incl.photo-z)	30	$1.98^{+0.04}_{-0.06}$	261/165
NL AGN	7	$1.64^{+0.11}_{-0.11}$	37/32
NL AGN (incl.photo-z)	18	$1.50^{+0.08}_{-0.08}$	144/75
Optically faint	8	$1.09^{+0.30}_{-0.30}$	9/8

of the counts in the 0.5-8 keV band we find  $\Gamma = 1.49 \pm 0.06$ . Note however, that the exclusion of the sources with a large number of photons may introduce a bias against the sources with a soft spectrum. This is because of the large effective area of the EPIC CCD detectors at soft energies implying that a large number of photons in the total band is most likely owing to a large number of photons at soft energies (0.5-2 keV).

The co-added spectrum of the 24 spectroscopically confirmed BL AGN gives  $\Gamma = 2.02^{+0.04}_{-0.05}$ . Although there are a few BL AGN with significant photoelectric absorption, as demonstrated above, their contribution to the co-added BL AGN spectrum is minimal. When we add the above 24 sources to the 6 (spectroscopically unidentified) sources which appear point-like on optical images and present blue colours, and hence are candidate QSOs, we obtain  $\Gamma = 1.98^{+0.04}_{-0.06}$ . The 7 NL/AL AGN have a flatter spectrum  $\Gamma = 1.64 \pm 0.11$ . When we include the 11 nearby AGN (extended in the optical with red colours), we obtain a spectrum of  $\Gamma = 1.50^{+0.08}_{-0.08}$ , similar to the spectrum of the X-ray background at these energies. Finally, the 8 'optically faint' sources i.e. those which have no optical counterparts in the SDSS, have a very flat spectrum (albeit with large uncertainties),  $\Gamma \approx 1.1 \pm 0.3$  suggesting large amounts of obscuration.

## 6 DISCUSSION

The *XMM-Newton*/2dF survey provides the opportunity to explore in detail the sources which are responsible for a large fraction of the XRB (about 50 per cent at the flux limit of our survey  $f_{2-8\text{keV}} \approx 10^{-14} \text{ erg cm}^{-2} \text{ s}^{-1}$ .)

The hardness ratio distribution provides some initial information on their X-ray spectral properties. The population synthesis models (e.g. Comastri et al. 2001) predict that about two thirds of the 2-10 keV X-ray selected sources with a flux higher than  $f_{2-10\text{keV}} > 10^{-14} \text{ erg sec}^{-1} \text{ cm}^{-2}$  should present a *rest-frame* column  $> 10^{22} \text{ cm}^{-2}$ , (roughly one third should have  $N_{\text{H}} > 10^{23} \text{ cm}^{-2}$ ). From Fig. 6 (upper panel), where the distribution of the rest-frame column densities are plotted for the spectroscopically identified sources, it appears that a very small fraction of the sources have columns  $N_{\text{H}} > 10^{22} \text{ cm}^{-2}$ . A deficit of strongly absorbed sources has also been noticed in the bright *XMM-Newton* samples of Piconcelli et al. (2002) and Caccianiga et al. (2004). In Fig.6 (lower panel) we plot the rest-frame column density distribution for all sources (including those with photometric redshift). We see that only about 20 and 3 per cent of our sources have a column density higher than  $10^{22}$  and  $10^{23}$

$\text{cm}^{-2}$  respectively in disagreement with the standard population synthesis models.

We further explore the spectral properties of the hard X-ray sample as a function of X-ray flux. Even at the relatively faint flux levels probed here the average spectrum of all sources ( $\Gamma \approx 1.8$ ) is much steeper than the spectrum of the XRB in the 2-10 keV band  $\Gamma \approx 1.4 - 1.5$  (e.g. Gendreau et al. 1995; Miyaji et al. 1998). This may be due to a few bright sources that dominate the total counts thus contaminating the average spectrum. Excluding the 9 brighter sources which contribute about 60 per cent of the total source counts, we obtain a flatter spectral index with  $\Gamma \approx 1.6$ . The hardening of the spectral index above, with the exclusion of the 9 bright sources, could represent a trend where harder (more absorbed) sources are detected with decreasing flux. However, when we divide our sample into two 2-8 keV flux bins we find no evidence for spectral hardening. We obtain  $\Gamma = 1.75 \pm 0.06$  (49 objects) and  $\Gamma = 1.81 \pm 0.06$  (12 objects) for the sources with flux  $10^{-14} < f_{2-8\text{keV}} < 10^{-13}$  and  $f_{2-8\text{keV}} > 10^{-13} \text{ erg cm}^{-2} \text{ s}^{-1}$  respectively. The above conclusion is further supported by inspection of Fig. 5 where the hardness ratios are plotted as a function of the 2-8 keV flux. Apart from the 3 brightest sources which present steep spectra there is no obvious evidence for the hardening of the hardness ratio with decreasing flux. This is naturally explained as the absorbing columns are not large enough to significantly affect the 2-8 keV band (but can affect the soft 0.5-2 keV and thus the total 0.5-8 keV band, see e.g. Tozzi et al. 2001, Alexander et al. 2003). Thus, there is no marked evolution of the hardness ratio in the 2-8 keV band, at least in the limited flux range probed by our survey. However, we note that at least two deeper X-ray surveys appear to find evidence for a weak evolution of the hardness ratio with the hard band flux (Harrison et al. 2003, Fiore et al. 2003 but cf. Tozzi et al. 2001) suggesting that a number of sources with higher column densities may be detected at fluxes fainter than the limit of our survey.

As we have identifications for a large fraction of our sources, we can explore the spectral properties of individual classes of sources. Out of the 61 detected sources 31 have been spectroscopically identified with AGN. Among the subsample of hard X-ray sources with redshifts we find (i) 24 BL AGN (ii) 7 AGN exhibiting narrow emission or absorption lines. The majority of these sources are BL AGN. As many of our identifications come from the 2QZ and the SDSS surveys which are primarily tuned toward the detection of UV excess QSOs, the large number of BL AGN found so far among the spectroscopically identified sources is not surprising. For a large number of our sources we do not have spectra. However, we can obtain some information on their nature from their optical colours plotted in Fig. 4. The 25 unidentified sources comprise a mixture of (i) 6 point-like sources in the optical most of which are likely to be QSOs (ii) 11 optically extended sources with primarily red colours suggesting low- $z$  galaxies associated with nearby either obscured or low luminosity AGN (iii) 8 sources with no optical counterpart.

We attempt to constrain the co-added spectral properties of the above populations to explore whether they are consistent with those of the XRB. For the 24 BL AGNs the average spectrum is steep having a power-law photon in-

dex  $\Gamma = 2.02_{-0.05}^{+0.04}$ . The addition of the 6 probable QSOs for which we have determined photometric redshifts yields again a comparable steep spectrum  $\Gamma \approx 1.98$ . Detailed spectral fits of individual sources reveal only two BL AGN with non-negligible rest-frame absorbing column densities ( $> 10^{22} \text{ cm}^{-2}$ ). Note that although there have been many claims for the detection of BL AGN at moderate to high redshift with significant absorbing columns only a limited number of cases are based on spectral fits (e.g. Reeves & Turner 2000; Georgantopoulos et al. 2003; Brusa et al. 2003).

The average spectrum of the 7 NL/AL AGN is somewhat flatter than that of BL AGN ( $\Gamma \sim 1.6$ ). The addition of the 11 galaxies with red colours, to the above sample results to an average spectrum of  $\Gamma \sim 1.5$  similar to the spectrum of the XRB in this band. Interestingly, the individual fits to the spectra of the 7 spectroscopically identified NL/AL AGN do not exhibit significant excess X-ray absorption above the Galactic. This can be explained if some of these are relatively weak AGN where the optical nuclear light is diluted by the strong galaxy component (e.g. Georgantopoulos et al. 2003, Severgnini et al. 2003, Maiolino et al. 2003).

Finally, the 8 'optically faint' sources, namely those which have no optical counterpart at the limit of the SDSS, present a very flat spectrum, albeit with large uncertainty ( $\Gamma \approx 1.1 \pm 0.3$ ). Obscured QSOs at high redshift may be associated with the last subclass of sources. Indeed, at high redshift the flux observed in the optical band originates in rest-frame UV wavelengths, which are most sensitive to reddening. However, even if all 8 sources which have no optical counterpart, were associated with obscured QSOs, this number would still be too small to be consistent with the 3/1 ratio of obscured to unobscured AGN observed in the local Universe.

## 7 CONCLUSIONS

We are reporting on the X-ray spectral properties of the hard X-ray selected sample detected in the *XMM-Newton*/2dF survey which covers about  $1.6 \text{ deg}^2$ . 61 sources have been detected in the 2-8 keV band down to a flux limit of  $f \approx 10^{-14} \text{ erg cm}^{-2} \text{ s}^{-1}$ . At this flux, our sources contribute about 50 per cent of the XRB in the 2-8 keV band. Spectral identifications exist for 34 sources (these produce about 30 per cent of the X-ray background) while photometric redshifts have been determined for another 17 sources which are most probably AGN. 8 sources have no optical counterpart to the photometric limit of the SDSS survey ( $r \approx 22.5$ ). The main conclusions can be summarised as follows:

(i) The majority (24) of the spectroscopically identified sources are BL AGN. However, this may be attributed to the fact that a fraction of our spectral classification comes from the cross-correlation of our catalogue with the 2QZ and the SDSS surveys which primarily detect UV excess QSOs. 7 sources are identified as NL (or AL) AGN on the basis of the lack of broad emission lines in the optical spectra. Among the sources with no spectroscopic classification, 6 are point-like with blue colours and are most probably QSOs. Another 11 are associated with optically extended sources with primarily red colours, suggesting that these are most likely nearby AGN.

(ii) The average spectrum of all sources is represented

by a power-law with a steep photon index of  $\Gamma \approx 1.8$ . When we exclude the 9 brighter sources, in terms of the number of counts in the total band, we obtain  $\Gamma \approx 1.5$ . The hardness ratio distribution shows a deficit of strongly absorbed sources ( $N_{\text{H}} > 10^{22} \text{ cm}^{-2}$ ) in disagreement with the standard population synthesis models.

(iii) The average spectrum of the 24 BL AGN is steep ( $\Gamma \approx 1.9$ ). However, there at least two BL AGN which present large ( $N_{\text{H}} > 10^{22} \text{ cm}^{-2}$ ) amounts of absorption, as shown from the detailed spectral fits. Although these present great interest for the physics of AGN, it appears that they do not form a substantial fraction of the QSO population.

(iv) The spectrum of the 7 NL/AL AGN, is flatter with  $\Gamma \sim 1.6$ . When we add to the above, the 11 spectroscopically unidentified sources which are optically extended and present red colours, and thus are also probably associated with nearby NL AGN, we obtain a similar spectrum  $\Gamma \approx 1.5$ .

(v) The spectrum of the 8 sources which have no optical counterpart is very flat, suggesting that these may be associated with obscured AGN at high redshift.

## 8 ACKNOWLEDGMENTS

This work is jointly funded by the European Union and the Greek Government in the framework of the programme "Promotion of Excellence in Technological Development and Research", project "X-ray Astrophysics with ESA's mission XMM".

We acknowledge use of the 100k data release of the 2dF Galaxy Redshift Survey. The 2dF QSO Redshift Survey (2QZ) was compiled by the 2QZ survey team from observations made with the 2-degree Field on the Anglo-Australian Telescope.

Funding for the creation and distribution of the SDSS Archive has been provided by the Alfred P. Sloan Foundation, the Participating Institutions, the National Aeronautics and Space Administration, the National Science Foundation, the U.S. Department of Energy, the Japanese Monbukagakusho, and the Max Planck Society. The SDSS Web site is <http://www.sdss.org/>. The SDSS is managed by the Astrophysical Research Consortium (ARC) for the Participating Institutions. The Participating Institutions are The University of Chicago, Fermilab, the Institute for Advanced Study, the Japan Participation Group, The Johns Hopkins University, Los Alamos National Laboratory, the Max-Planck-Institute for Astronomy (MPIA), the Max-Planck-Institute for Astrophysics (MPA), New Mexico State University, University of Pittsburgh, Princeton University, the United States Naval Observatory, and the University of Washington.

## REFERENCES

- Alexander, D.M., Brandt, W.N., Hornschemeier, A.E., Garmire, G.P., Schneider, D.P., Bauer, F.E., Griffiths, R.E., 2001, *AJ*, 122, 2156  
 Alexander, D.M. et al. 2003, *AJ*,  
 Almaini, O., Boyle, B. J., Griffiths, R.E., Shanks, T., Stewart, G.C., Georgantopoulos, I., 1995, *MNRAS*, 277, L31  
 Baldi A., Molendi S., Comastri A., Fiore F., Matt G., Vignali C., 2002, *ApJ*, 564, 190

- Barger A. J., Cowie L. L., Brandt W. N., Capak P., Garmire G. P., Hornschemeier A. E., Steffen A. T., Wehner E. H., 2002, *AJ*, 124, 1839.
- Boyle, B.J., Georgantopoulos, I., Blair, A.J., Stewart, G.C., Griffiths, R.E., Shanks, T., Gunn, K.F., Almaini, O., *MNRAS*, 296, 1
- Brandt W. N., 2001, *AJ*, 122, 2810
- Brusa M. et al., 2003, *A&A*, 409, 65
- Caccianiga, A. et al. 2004, *A&A*, in press, astro-ph/0312344
- Cash W., 1979, *ApJ*, 228, 939
- Colless M., Dalton G., Maddox S. et al., 2001, *MNRAS*, 328, 1039
- Comastri A., Setti G., Zamorani G., Hasinger G., 1995, *A&A*, 296, 1
- Comastri, A., Fiore, F., Vignali, C., Matt, G., Perola, G.C., La Franca, F., 2001, *MNRAS*, 327, 781
- Croom, S.M., Smith, R.J., Boyle, B.J., Shanks, T., Loaring, N.S., Miller, L., Lewis, I.J., 2001, *MNRAS*, 322, L29
- Csabai, I. et al. 2003, *AJ*, 125, 580
- Dickey J. M., Lockman F. J., 1990, *ARA&A*, 28, 215
- Downes A. J. B., Peacock J. A., Savage A., Carrie D. R., 1986, *MNRAS*, 218, 31
- Fiore, F., et al., 2003, *A&A*, 409, 79
- Fukugita M., Ichikawa T., Gunn J. E., Doi M., Shimasaku K., Schneider D. P., 1996, *AJ*, 111, 1748
- Gendreau K., et al. 1995, *PASJ*, 47L, 5
- Georgakakis, A., Georgantopoulos, I., Stewart, G.C., Shanks, T., Boyle, B.J., 2003, *MNRAS*, 344, 161
- Georgakakis, A. et al., 2004, *MNRAS*, in press, astro-ph/0311609
- Georgantopoulos, I., Stewart G. C., Shanks T., Boyle B. J., Griffiths R. E., 1996, *MNRAS*, 281, 71
- Georgantopoulos I., Stewart G. C., Blair A. J., Shanks T., Griffiths R. E., Boyle B. J., Almaini O., Roche N., 1997, *MNRAS*, 291, 203
- Georgantopoulos, I., Almaini, O., Shanks, T., Stewart, G.C., Griffiths, R.E., Boyle, B.J., Gunn, K.F., 1999, *MNRAS*, 305, 125
- Georgantopoulos, I., Zezas, A., Ward, M.J., 2003a, *ApJ*, 584, 129
- Georgantopoulos, I., Georgakakis, A., Stewart, G.C., Akylas, A., Boyle, B.J., Shanks, T., Griffiths, R.E., 2003b, *MNRAS*, 342, 321
- Giacconi R., et al. 2002, *ApJS*, 139, 369
- Gilli R., Risaliti G., Salvati M., 1999, *A&A*, 347, 424
- Giommi P., Perri M., Fiore F., 2000, *A&A*, 362, 799
- Harrison, F.A., Eckart, M.E., Mao, P.H., Helfand, D.J., Stern, D., 2003, *ApJ*, 596, 944
- Hatziminaoglou, E., Mathez, G. Pello, R., 2000, *A&A*, 359, 9
- Kim, D.W., et al. 2004, *ApJS*, 600, 59
- Maiolino, R. et al. 2003, *MNRAS*, 344, L59
- Miyaji T., Ishisaki Y., Ogasaka Y., Ueda Y., Freyberg M., J. Hasinger G., Tanaka Y., 1998, *A&A*, 334, L13
- Mushotzky R. F., Cowie L. L., Barger A. J., Arnaud, K. A., 2000, *Nature*, 404, 459
- Piconcelli, E., Cappi, M., Bassani, L., Fiore, F., di Cocco, G., Stephen, J. B., 2002, *A&A*, 394, 835
- Reeves, J., & Turner, M., 2000, *MNRAS*, 316, 234
- Severgnini P. et al., 2003, *A&A*, 406, 483
- Shanks, T., Georgantopoulos, I., Stewart, G.C., Pounds, K.A., Boyle, B.J., Griffiths, R.E., 1991, *Nat*, 353, 315
- Stoughton C., et al., 2002, *A&AS*, 34, 1288
- Strüder L., Briel U., Dennerl K., et al. 2001, *A&A*, 365, L18
- Tozzi P., et al., 2001, *ApJ*, 562, 42
- Turner M. J. L., Abbey A., Arnaud M., et al., 2001, *A&A*, a365, L27
- Ueda Y., et al., 1998, *Nat*, 391, 866
- Ueda, Y. et al., 1999, *ApJ*, 518, 656
- York D. G., et al., 2000, *AJ*, 120, 1579